

FLOWCAM ANALYSIS OF THE OCEAN LITHOGENIC PARTICLES DURING THE 2021 VOLCANIC ERUPTION OF LA PALMA, CANARY ISLANDS



Eduardo Augustin Baixas

Marine Sciences Degree

4th Academic Year

Academic supervision by:

Inmaculada Menéndez

Aja Trebec

Final Degree Project

**FLOWCAM ANALYSIS OF THE OCEAN LITHOGENIC PARTICLES
DURING THE 2021 VOLCANIC ERUPTION OF LA PALMA,
CANARY ISLANDS**

STUDENT: Eduardo Augustin Baixas

DEGREE: Degree in Marine Sciences

SUPERVISOR/TUTOR: Inmaculada Menéndez González

CO-TUTOR: Aja Trebec

DEPARTMENT: Physics, University of Las Palmas of Gran Canaria (ULPGC), Spain

COMPANY: Instituto Universitario de Oceanografía y Cambio Global (IOCAG) – Grupo Geología Aplicada y Regional (GEOGAR)

Front image source: <https://www.eldia.es/la-palma/2022/06/09/tuberia-fajana-volcan-palma-propuesta-67068561.html>

INDEX

ABSTRACT	3
1. INTRODUCTION	4
1.1 - Lithogenic and biogenic fluxes	4
1.2 - Lithogenic flux in the Canary basin, Saharan dust	4
1.3 - Special input during volcanic eruptions of lithogenic fluxes in the Canary basin	5
1.4 - Flow imaging microscopy using FlowCAM®	5
1.5 - Objectives	5
2. GEOLOGICAL SETTING	6
3. MATERIALS AND METHODS	7
3.1 - Sample collection	7
3.2 - Sample processing and particle image analysis using FlowCAM®	8
3.3 - Imaging analysis	9
3.4 - Volcanic ashes and saharan dust standards	9
3.5 - Parameter characterization	11
4. RESULTS	12
5. DISCUSSION	15
6. CONCLUSIONS	16
ACKNOWLEDGEMENTS	17
REFERENCES	18

ABSTRACT

Lithogenic flux (mineral particles), plays a key role in the oceanic fluxes, as nutrient and its ballast effect. Lithogenic flux in the Canary basin is mainly Saharan dust. In September 2021, a volcanic eruption struck in La Palma Island, reaching the coast, which contributed substantially with a fresh volcanic ash oceanic flux input. Flow imaging microscopy uses digital images to measure the size and shape of each particle. FlowCAM® was utilized to measure large numbers of diatom valves in an automated manner. However, FlowCAM® has still not been applied to lithogenic particle studies, despite its great potential for image identification analysis. Thousands of particle images are captured per second by the camera which includes all the spectrum of organic and mineral particles, allowing a precise visualization of the lithogenic particles.

Particle samples were obtained during an oceanographic campaign (PLOCAN/ULPGC campaign) close to the new lava delta (28°36'N-17°55'W) using Niskin bottles (at depths from 5 to 20 m, collected into glass bottles and preserved with formol acetic acid). Two pattern samples, one of Saharan dust and another of volcanic ash, from the recent eruption of La Palma, were analyzed previous to the particle evaluation for a more realistic identification. A mineral identification of La Palma ashes (particles composed of 75% vitreous and 25% pyroxene and olivine) and Saharan dust (45% quartz, 25% carbonates, 15% feldspars, and 10% Mn-Fe oxides) was incorporated to the study. A specific software was used to characterize the oceanic water particles into different classes based on grain size distribution as the main criterion. Particle concentration, transparency, roughness, and edge gradient particle parameters were obtained consequently as secondary criteria.

This study demonstrates the effectiveness of FlowCAM® analysis for textural studies of oceanic lithogenic particles. Observed results showed a mix of both volcanic ash and Saharan dust grain size distribution patterns constituted the lithogenic flux particle samples, yet these tend to resemble more the Saharan dust pattern.

KEYWORDS: Lithogenic flux particles, volcanic flux input, flow imaging microscopy, La Palma 2021 volcanic eruption.

1. INTRODUCTION

1.1 - Lithogenic and biogenic fluxes composition

Particulate organic matter in the ocean is composed of living organisms and non-living organic matter (detritus) which can be described as the bulk in terms of carbon, besides other components of inorganic matter (skeletons or shells), which form the particles of the biogenic fluxes (Dong et al. 2010). On the other hand, the particles of the lithogenic fluxes are composed of natural mineral particles (NMP) and consist of the sinking terrigenous particles in the oceanic waters. In many regions of the ocean, lithogenic matter is a major component of particle flux to the deep-sea (Ratmeyer et al. 1998). Lithogenic particles enter marine environments through fluvial and aeolian transport. Fluvial processes contribute, by far, to the largest amounts of mineral detritus in the oceans (Milliman and Syvitski, 1992).

The plankton community structure is closely related to the composition of biogenic matter. Diverse microplanktonic organisms such as coccolithophorids (Sprengel et al. 2000), diatoms (Huskin et al. 2004, Anabalón et al. 2014), foraminifera (Elder et al. 2018), and mesoplanktonic animals such as crustaceans and mollusca (e.g., gastropods) are amongst the particulate components that compose the oceanic mineral biogenic flux. The microplanktonic and mesoplanktonic communities produce shells of carbonate (coccolithophorids, foraminifera), silica (diatoms), or chitin as exoskeletons (crustaceans). Transparent exopolymer particles (TEPs) and fecal matter are also considered as major components of particulate organic carbon (POC). These compounds are all expected to sink, generating what is known as the biological pump, a principal mean of vertical transport of carbon in the ocean, and the sinking of POC is one of its main components (Buesseler et al. 2007).

1.2 - Lithogenic flux in the Canary basin, Saharan dust

Dust source in the Canary basin is predominantly allochthonous, the Saharan dust, from the neighboring African continent transported during haze conditions. Sources of autochthonous origins also exist (particles generated and/or recycled within the insular area). The Canary Islands are in the proxy area of most paths of Saharan aerosol fluxes, which makes this region an ideal place to study this phenomenon. The Saharan desert generates a wide variety of particles owing to a range of different origins (magmatic, sedimentary, and metamorphic) and ages (from Precambrian to Recent) present in Northwest Africa (Piqué 2001). The source of the dust components was established, to be in two major areas: the Bodélé depression (Southern of Chad) and the Eastern Mauritania – Western Mali – Southern Algeria area (Goudie and Middleton, 2001; Menéndez et al., 2007). Saharan dust is the major source of lithogenic fluxes input on the Canary Basin. Throughout the atmospheric lifetime, the dust particles are subject to mixing and ageing. These actions bring significant changes in the molecular composition of

the airborne particles before their removal from the atmosphere on the ocean surface. The dry climate of the area and the seasonal presence of the Saharan Air Layer in the Canary Basin promotes a connection between the Sahara Desert and the Canary Current in terms of lithogenic input (Menéndez et al., 2017). The trade winds are effective transporters of aeolian dust blow mainly from NE, ENE, and NNE at an average speed of 6 m/s; these winds are more effective from June to September (Sangrá et al., 2009).

1.3 - Special input during volcanic eruptions of lithogenic fluxes in the Canary basin

Volcanic ash enters the ocean as terrigenous material, either through coastal dynamics or aeolian transport. As ash infiltrates the water column, it momentarily provides local fertilization at the entered region (Gómez-Letona et al. 2018). A particular case would be the earliest instants of a volcanic eruption where the material is fresh therefore it has not been altered, or has been altered in the slightest, and is very texturally fragmented. Due to the immediate dissolution of adsorbed components (phosphate, iron, silicon and manganese), when recently erupted volcanic ash comes in contact with the ocean surface water, macronutrients and bioactive trace metals are released with enough speed to become available to provision primary producers (Frogner et al. 2001).

1.4 - Flow imaging microscopy using FlowCAM®

FlowCAM® is an imaging cytometry tool that was originally developed for use in aquatic sciences utilized to provide a more rapid and unbiased method of enumerating, measuring and classifying large numbers of phytoplankton in an automated manner (Spaulding et al. 2012; Bishop and Spaulding 2017; Poulton 2016). However, FlowCAM® has still not been applied to lithogenic particle studies, despite its great potential for image analysis identification. Thousands of particle images are captured per second by the camera which includes all the spectrum of organic and mineral particles, allowing a precise visualization of the lithogenic particles. The instrument stores a digital image of each particle along with real time fluorescence and size measurements, allowing rapid characterization of populations. Flow imaging microscopy is a solution-based technique to capture subvisible and visible images in a microfluidic channel under flow (<https://www.fluidimaging.com/particle-analysis>).

1.5 - Objectives

The main aims in this final degree project include: The identification and classification of lithogenic particles produced during the 2021 Tajogaite volcano eruption in the Cumbre Vieja region of La Palma Island. Testing the FlowCAM® capability of lithogenic particle

identification and imaging. And lastly, analyzing the potential of Saharan dust and volcanic ash as FlowCAM® standards.

2. GEOLOGICAL SETTING

The La Palma Island is located off the West coast of North Africa, in the Canary archipelago, situated in the Macaronesia volcanic province, in the African oceanic plate of the Central Atlantic (Fig.1a). The archipelago, along with other islands and submarine mountains, is associated to an anomaly in the lower mantle, a plume that has given rise to several hotspots within the plate which have developed persistent submarine and subaerial vulcanism since the Cretaceous until now (Mangas, 2022). The emersion of La Palma Island took place during the Plio-Quaternary (<4 Ma; Schmincke and Sumita 2010). It emerged with the formation of Garafía and the Taburiente shield volcanoes (1.7-0.4 Ma) (Fig. 1b), Cumbre Nueva rift (850–560 ka) and the Bejenado complex (490–560 ka). Successively, the island’s vulcanism spread southwards forming the Cumbre Vieja rift (ca. 125 ka), that hosts the Tajogaite volcanic system (Fig. 1c and d) in La Palma (Carracedo et al. 2001). A week before September 19th, 2021, a notable cortical bulging in the Cumbre Vieja ridge region of the island was notified. Subsequently, and after 50 years of quiescence a seismic swarm unbound a volcanic eruption in the newly named Tajogaite volcano (Fig. 2). While active, until December 14th, 2021, thousands of earthquakes and magma flow occurred. Post eruptive activity was also registered which included a few daily earthquakes, thermal anomalies and the degassing of hydrothermal fluids from nearby craters and fissures (Pankhurst et al., 2022). The lava and tephra composition of the volcanic eruption was basanitic (Carracedo et al. 2022).

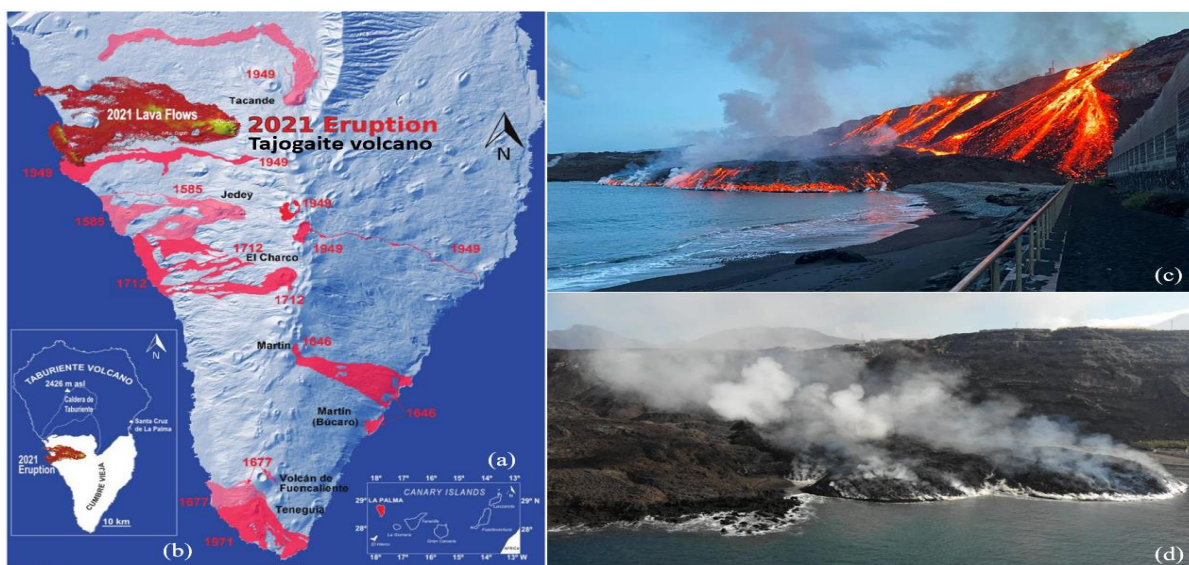


Figure 1. (a) Location of the La Palma Island and Tajogaite volcano eruptions and (b) historical eruptions including the Taburiente volcano and the formation of Cumbre Vieja (modified from Carracedo et al., 2022); (c) and (d) images of the active Tajogaite volcanic system and the formation of lava deltas from a terrestrial and an aerial point of view respectively.

The eruptive process was characteristic of a strombolian type, with punctual phreatomagmatic phases where lava flows were predominant along with falling pyroclasts and magmatic gases which had a minor impact. The volume of emitted materials during the eruption reached around $156 \cdot 10^6 \text{ m}^3$, the area occupied by the lava was of 1219 ha and 73.8 km of public roads were affected. The surface reclaimed from the sea in the coastal lava platforms has been of 50 ha approximately forming two lava deltas, a larger one South of the abrasion platform and a much smaller one North of the same platform (Fig. 2). Samples were gathered in an area close to the bigger delta. Other historical eruptions in the island such as the 1712, 1949 and 1971 eruptions had the same effect on the island's coastal system, these events also provoked the formation of lava deltas (Fig. 1b; Carracedo et al. 2022).



Figure 2. Volcanic region of La Palma Island (modified from Carracedo et al., 2022). The yellow oval indicates the ocean sampling area of the ULPGC-PREVOLCA campaign for this lithogenic particle study.

3. MATERIALS AND METHODS

3.1 - Sample collection

Particle samples were obtained during an oceanographic PLOCAN/ULPGC campaign on the coast of to the new delta lava (Fig 2), using Niskin bottles at depths from 5 to 20 m, collected into glass bottles and preserved with formol acetic acid. A total of 22 samples were collected of which 4 were selected for the purposes of this study at 5, 10 and two at 20 m separately.

3.2 - Sample processing and particle image analysis using FlowCAM®

Samples were taken into a IOCAG lab of the Biological Oceanography Group (GOB, IOCAG; <https://iocag.ulpgc.es/research/research-units/gob>), where the FlowCAM® is installed. Previous to the analysis, 250 ml of sample are filtered through a 280 µm mesh. The filtered volume is not specific, every project decides based on the needs and available material. Filtered samples are then fixated using 5 ml of a 50% formol + 50% glacial acetic acid solution. Next, 100 ml of the sample are sedimented into the Utermöhl chamber for 24 hours. Later, the sample is transferred to the FlowCAM® where 5 ml are filtered through a 200 µm mesh before entering the machine.

The liquid sample containing the particles streams through the flow cell past the microscope optics at 0.150 ml/min. The microscope uses a x10 lens and thousands of particle images are captured per second by the camera. Images are shown in the VisualSpreadsheet (<https://www.fluidimaging.com/products/particle-analysis-software-5>) software where each particle can be visualized individually. The internal structure of the FlowCAM® (Fig. 3) is relatively simple and is directly connected to a computer. It consists of an entering unit at the top where the filtered sample is added (Fig. 3a), a flow cell with a microscope and a camera where the images are taken (Fig. 3b), followed by a water pump (Fig. 3c) that moves water out of the cell and inside the waste container (Fig. 3d).

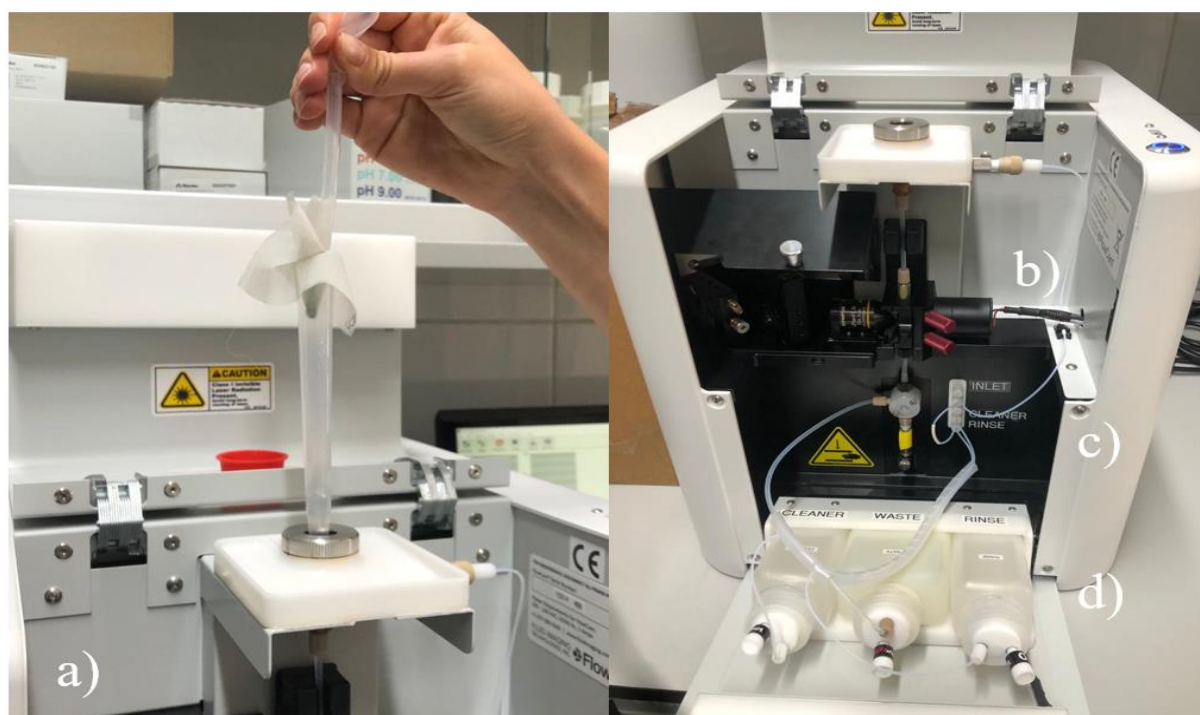


Figure 3. FlowCAM® internal structure. (a) sample input after filtration through a 200 µm mesh. (b) Flow cell and microscope optic components. (c) Water pump. (d) Waste containers.

Standard samples of Saharan dust and volcanic ash from La Palma volcano were analyzed previous to the final water sample analysis for a better understanding of which particles were of interest.

3.3 - Imaging analysis

VisualSpreadsheet was employed to characterize the oceanic water particles into 23 different classes, based on particle diameter as the main criterion. Different classes were created for every 5 μm diameter variation starting at 10 μm . Before the particles from the water samples were classified, 23 different libraries were created with the same criterion using the images from the two standard samples of volcanic ash and Saharan dust. Library creation helps the software run an auto classification as it uses the information given to find the particles of interest within the thousands of images. Classes were thoroughly checked for any auto-classification errors that might have occurred as some libraries lacked information and therefore were unusable. Moreover, the software frequently auto-classified particles that were not of interest as, in this case, it was instructed to classify by diameter, therefore non-lithogenic particles or blurry images were likely to appear. Area, circularity, edge gradient, perimeter, roughness, abundance, and transparency parameters were obtained consequently for each individual particle as secondary criteria. Data was exported into an Excel sheet to facilitate a comparison of the studied parameters for each particle. Particles of interest were chosen based on this data for each criterion.

3.4 - Volcanic ashes and Saharan dust standards

The main mineralogical composition of the volcanic tephra and lavas from La Palma eruption which formed the lava deltas is basanitic pyroxenic olivinic, and is composed of 75 - 83% vitreous material and 17 - 25% phenocrysts and microphenocrysts minerals (pyroxene, olivine, amphibole, plagioclase, and Fe Ti oxides (Fig 4. Ancochea, 2022). Within the mineral population, pyroxene is predominant (60 - 65%), followed by olivine (22 - 30%), plagioclase and Fe Ti oxides (3 - 15% and 6 -12% respectively), and lastly the amphibole which is the rarest (<1.5%).

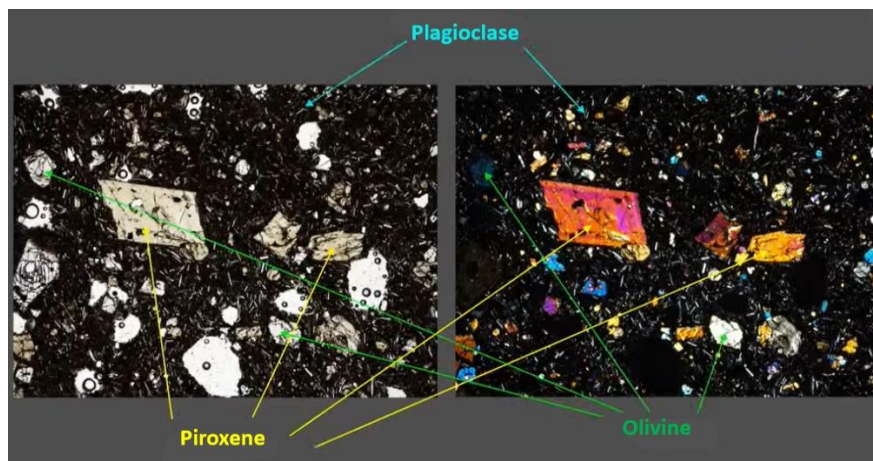


Figure 4. Lava thin section under petrographic microscope with plain light (left) and cross-polarized light (right). The vitreous material appears in black. With plain light, pyroxene is the most translucent while olivine and plagioclases are more transparent (modified of Ancochea 2022).

Saharan dust displays a bimodal curve (Fig. 5a) with a main mode of 16 μm approximately, negative skewness with a tail on finer fractions peak and a coarser silt fraction mode (Fig. 5a; Menéndez et al., 2009). The lithogenic particles shows a mean grain size distribution (Fig. 5b) around 22 μm , although it becomes distinctively coarser during Saharan dust events, increasing up to 57 μm (Baez et al., 2019). Saharan dust mineralogy is mainly composed of 45% quartz, 25% carbonates, 15% feldspars, and 10% Mn-Fe oxides; (Fig. 5c; Menéndez et al., 2007). Once Saharan dust goes through the ocean water column, the original aeolian mineralogy becomes identifiable (e.g., quartz) as lithogenic flux (Fig. 5d; Jaramillo et al., 2016).

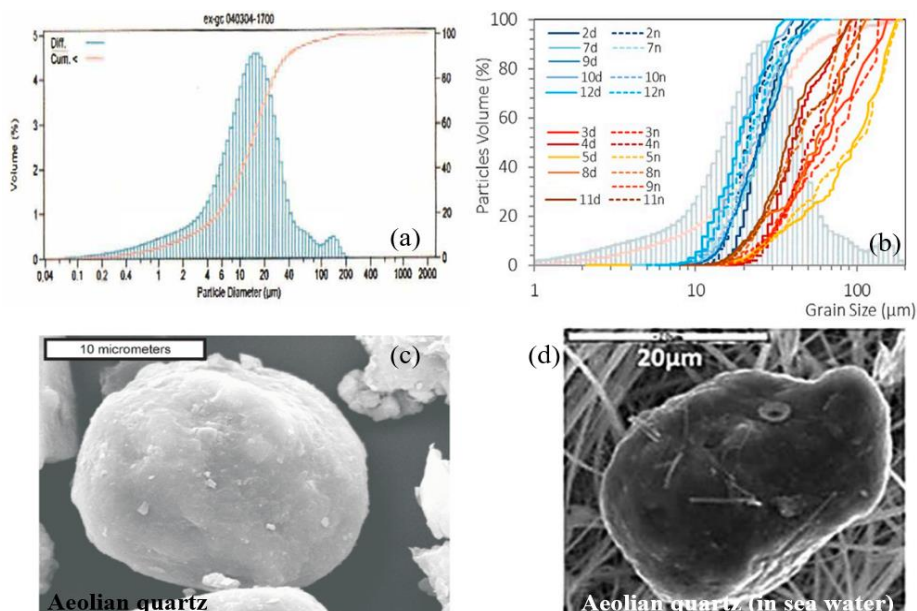


Figure 5. Grain size distribution examples of (a) Saharan dust (Menéndez et al., 2009) and (b) lithogenic fluxes in Canary Basin (Baez et al., 2019); aeolian quartz examples of (c) Saharan dust, aeolian quartz (Menéndez et al., 2007) and (d) lithogenic flux particle from the Canary Basin, aeolian quartz after going through the water column (Jaramillo et al., 2016).

3.5 - Parameter characterization

The graphic parameters extracted from VisualSpreadsheet for their analysis were: circularity, transparency, roughness, and edge gradient. Ranging values for each individual parameter were obtained from the found maximums and minimums within all samples and patterns during their analysis for this study specifically.

Circularity ranged from 0.00 to 0.98. Values closer to 1 suggest a circular particle whereas lower values indicate the particle has little to no circular nature (Fig. 6a). Transparency ranged from 0.00 to 0.76, being this the maximum registered for a single lithogenic particle found in the volcanic ash pattern. High transparency values indicate a more transparent particle whereas low values imply an opaquer particle (Fig. 6b). Roughness varied from 0 to a found maximum in the Saharan dust pattern of 2.6. Low roughness indicates a smooth, round particle, while a higher value represents a harsh, irregular particle (Fig. 6c). Edge gradient varied between a found minimum of 39 to a maximum of 248. Greater estimates of edge gradient represent lithogenic particles with a clear and easily detectable contour. On the other hand, inferior estimates correspond to lithogenic particles with a more diffuse and harder to identify contour (Fig. 6d).

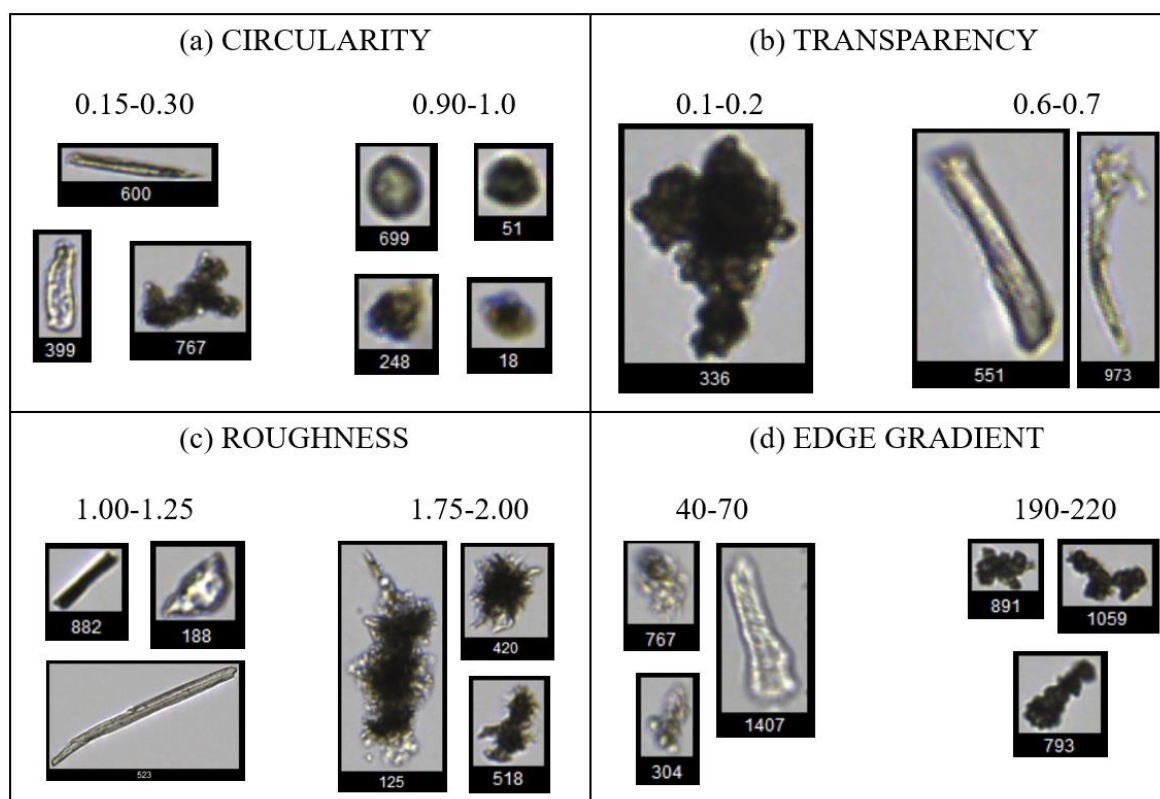


Figure 6. Examples of particles photographed during the flow imaging analysis of the samples and patterns studied to show a qualitative difference in (a) circularity, (b) transparency, (c) roughness, (d) edge gradient. A particle size scale is not given as sizes have been modified considering the displayed images are being used, in this case, for exhibit purposes only.

Regarding the statistical treatment of the samples, it is assumed that the particle populations follow a normal distribution pattern thus will be characterized using the mean, median, standard deviation (sorting), skewness, and kurtosis. These statistical elements are defined using the original logarithmic Folk and Ward graphical measures (Fig. 7) (Folk and Ward, 1957; Blott and Pye, 2001).

<p>(a) Mean</p> $M_Z = \frac{\phi_{16} + \phi_{50} + \phi_{84}}{3}$	<p>(b) Standard Deviation (sorting)</p> $\sigma_I = \frac{\phi_{84} - \phi_{16}}{4} + \frac{\phi_{95} - \phi_5}{6.6}$
<p>(c) Skewness</p> $Sk_I = \frac{\phi_{16} + \phi_{84} - 2\phi_{50}}{2(\phi_{84} - \phi_{16})} + \frac{\phi_5 + \phi_{95} - 2\phi_{50}}{2(\phi_{95} - \phi_5)}$	<p>(d) Kurtosis</p> $K_G = \frac{\phi_{95} - \phi_5}{2.44(\phi_{75} - \phi_{25})}$

Figure 7. Equations defining the statistical parameters studied. (a) Mean, (b) standard deviation (sorting), (c) skewness, and (d) kurtosis.

Sediment sorting is the degree of dispersion of a grain-size distribution around a central value (mean, median, or mode) (Mahiques et al., 2016). This parameter is used specifically in sedimentology studies and is equivalent to the standard deviation. Edge gradient and roughness were analyzed altogether because if edge gradient values are low, then roughness parameter estimates become unreliable as the contour of the particles would not be properly visible.

4. RESULTS

Ocean lithogenic particle concentration oscillates from 94 to 199 (particles/ml) where the intermediate values appear in the deeper samples and the superficial samples represent the range limits (Table 1). Mean grain size, median and sorting values in the ash and dust patterns range from 13.9 to 27.6 μm , 13.3 to 26.4 μm and from 8.5 to 21.0 μm respectively. In the case of the lithogenic particle samples these three parameters do not vary considerably and represent intermediate values within the obtained range. The ash and dust patterns presented skewness and kurtosis values ranging from 0.3 to 0.2 and 0.8 to 1.1, respectively. Lithogenic particles at

20 m depth showed similar skewness values to the Saharan dust and volcanic ash patterns, although it was greater at 5-10 m depth. Kurtosis values extend among the mesokurtic pattern range.

Table 1. Data obtained by statistical treatment of the samples and patterns including the total number of particles, concentration (particles/ml), mean grain size(μm), median (μm), sorting (μm), skewness, and kurtosis.

	ASH	DUST	E_5	E_10	E1_20	E2_20
PARTICLES	7981	2397	479	269	322	436
CONCENTRATION	-	-	199	94	148	189
MEAN	13.9	27.6	20.7	23.8	21.2	21.5
MEDIAN	13.3	26.4	18.2	21.7	20.3	22.7
SORTING	8.5	21.0	16.6	18.9	14.8	15.1
SKEWNESS	0.3	0.2	0.5	0.4	0.2	0.3
KURTOSIS	0.8	1.1	1.0	1.2	0.9	1.0

Furthermore, the statistical grain size distribution parameters of the volcanic ash pattern show a distinct textural nature compared to the rest of the studied samples (Fig. 8b). However, the Saharan dust pattern displays great similarity with the more superficial lithogenic particle samples, at 5 and 10 m deep, clearly different to the deeper samples.

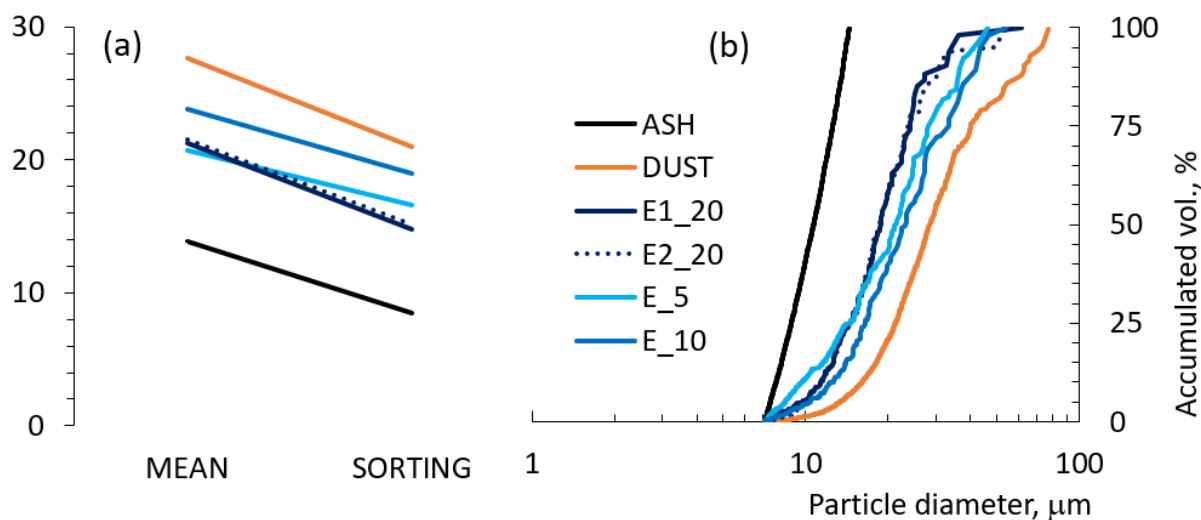


Figure 8. (a) Statistical analysis (mean and sorting) describing the grain size distribution of the analyzed patterns and samples, the y-axis corresponds to mean and sorting values; (b) Grainsize distribution of the volcanic ash, Saharan dust patterns, and lithogenic particle samples collected at La Palma coast at different depths.

As observed, the ash pattern is the most different to the rest of the samples since a fragmented distribution of the full pattern is represented. The volcanic ash population is much larger than the grain size range adapted for the rest of the samples. This volcanic ash fragment shows a small particle population between 9 and 11 μm . However, the grain size distribution of the Saharan dust in Canary Islands region follows a typical bimodal curve (Menéndez et al., 2009), with the exception of the fine grain tail due to the size restriction of the imaging analysis threshold. The total number of particles found and studied in the samples fluctuated between 269 and 479, whereas in the Saharan dust pattern 2397 particles were photographed and 7981 in the volcanic ash pattern. In addition, it is important to note that deeper samples are very similar, however, superficial samples are slightly different.

Mean transparency values range from 0.13 to 0.21 (Table 2). Both volcanic ash and Saharan dust patterns are less transparent than the lithogenic particles, being the dust pattern the least transparent with a mean of 0.13. Standard deviation is lower in the patterns meaning that the particles are more similar to each other than in the samples as these contain a mix of both patterns. Particle population was much larger in the patterns which contributes to obtain a lower standard deviation. The more superficial lithogenic particles (E_5 and E_10) are more transparent than sample E1_20. Lithogenic particle sample E_10 registered the highest transparency mean and median values of all the studied samples and patterns, although its standard deviation is, as well, the greatest.

Table 2. Mean and median lithogenic particle transparency of the studied samples and patterns, including standard deviation.

	ASH	DUST	E_5	E_10	E1_20	E2_20
MEAN	0.16	0.13	0.19	0.21	0.16	0.20
MEDIAN	0.18	0.15	0.22	0.25	0.18	0.23
SD	0.08	0.06	0.12	0.13	0.09	0.10

Roughness and edge gradient values were put alongside in the same table. The volcanic ash pattern shows the lowest mean roughness of 1.16 and particle sample E_10 the greatest, 1.32 (Table 3). Mean and median roughness values are higher in the lithogenic particle samples than in the volcanic ash and Saharan dust patterns except for the E1_20 sample mean roughness which turned out to be 0.01 lower than the Saharan dust pattern. Standard deviation is once again superior in the particle samples, apart from E1_20 which is equal to the volcanic ash pattern roughness standard deviation. Mean edge gradient is significantly larger in the volcanic ash pattern. Lithogenic particle samples show lesser mean and median edge gradient than both patterns.

Table 3. Mean and median edge gradient and roughness values obtained from the study of the lithogenic particle samples and patterns including the standard deviation.

	ASH	DUST	E_5	E_10	E1_20	E2_20
ROUGHNESS MEAN EDGE	1.16	1.20	1.24	1.32	1.19	1.28
GRADIENT MEAN	148.45	128.38	121.93	117.06	116.02	124.68
ROUGHNESS MEDIAN EDGE	1.13	1.16	1.18	1.26	1.16	1.22
GRADIENT MEDIAN	158.31	175.00	133.45	126.8	132.88	152.89
ROUGHNESS SD EDGE	0.12	0.13	0.20	0.30	0.12	0.24
GRADIENT SD	38.80	47.44	49.11	51.50	53.46	55.84

5. DISCUSSION

Saharan dust events sampled within hundreds of km from the source present a mean diameter of airborne particle amid 72 and 74 μm (Goudie and Middleton, 2001), while studies of dust transport over thousands of km from the source have measured mean diameter sizes between 1 and 30 μm (Goudie and Middleton, 2001). The data analysis performed in this study exhibited a mean grain diameter size of Saharan dust of $27.6 \pm 21.0 \mu\text{m}$, which coincides with the typical range. The Canary basin is in the middle of these two described distances; therefore, it is reasonable that the size distribution found is in between them.

The obtained mean grain size of the lithogenic particle samples of the La Palma lava delta was 22 μm . The superficial (10 m) particle grain size range in the canary basin is among 30 and 43 μm (Jaramillo et al., 2016). This range is greater than what was found in this study since the analyzed samples also contained volcanic ash particles which showed a mean diameter of $13.9 \pm 8.5 \mu\text{m}$, bringing down the overall mean grain size. Considering the grain size signature of Saharan dust in the Canary basin, more specifically in the studied oceanic lithogenic particles, as showed in Fig. 8, this value is consistent with the mean and median grain sizes of transported Saharan dust and the produced lithogenic particles in the northwest African coast, which commonly ranges between 5 and 30 μm in diameter (Goudie and Middleton, 2001; Holz et al. 2007).

Knowing the volcanic ash particles are smaller than the Saharan dust particles (Fig. 8b), it would fit that the deeper samples were alike the dust pattern because particles are larger and

the more superficial samples are closer to the volcanic ash pattern, nevertheless, this shows a change since samples collected at lower depths exhibit a grain size distribution curve closer to the volcanic ash pattern curve. Differences in the sinking rate occur between large and small particles. Smaller particles have a higher chance of being retained in the water column as a result of their low weight and density, whereas larger particles sink at a higher rate (Jaramillo et al., 2016). Lithogenic particles act as a ballast, supporting the vertical transport of biogenic aggregates to the deep ocean (Armstrong et al. 2002). When fresh volcanic ash meets the ocean surface water, macronutrients and bioactive trace metals become available to provision primary producers (Frogner et al. 2001), which could explain why, although being smaller particles, volcanic ash was more commonly found in deeper waters than the Saharan dust. These particles could be incorporated into organic aggregates, acting as ballast, and thus, increasing sinking (Armstrong et al., 2002).

Overall, taking into consideration the statistical parameters calculated (Table 1) as well as the mineralogy of the particles (Tables 2 and 3) and, most importantly, the standard deviation in all the lithogenic particle samples, it can be concluded that the studied samples contain a mix of both patterns yet tend to resemble more the Saharan dust pattern. The volcanic ash population was not properly analyzed because only the smaller particles could be photographed using the FlowCAM®, giving an incomplete grain size curve (Fig. 8b). Therefore, FlowCAM® analysis is not a reliable method for ocean lithogenic particle characterization regarding fresh volcanic ash particles although it is suitable for Saharan dust and oceanic lithogenic particle studies. With this work, the effectiveness to determine a vastly utilized pattern in sedimentology and paleoclimatology using FlowCAM® has been demonstrated. In addition, this pattern is basic in aeolian and marine sediment grain size distribution studies, obtaining contrastable results with other techniques and studies in the Canary basin and different latitudes (Van der Does et al., 2021).

6. CONCLUSIONS

In order to summarize the results obtained in this study, firstly, ocean lithogenic particle concentration varies from 94 to 199 particles/ml and the intermediate values appear in the deeper samples. Mean grain size, median and sorting estimates in the ash and dust patterns vary from 13.9 to 27.6 μm , 13.3 to 26.4 μm and from 8.5 to 21.0 μm , respectively. Nevertheless, for the lithogenic particle samples these three parameters do not vary greatly and correspond to intermediate values within the acquired range. The Saharan dust and the more superficial lithogenic particle samples are very similar and display a clear difference to the deeper samples. The volcanic ash pattern is the most different to the rest since only a fragmented distribution of

the full pattern is represented since the population is much larger than the studied grain size range. Finally, deeper samples are similar to each other, yet superficial samples are slightly different.

Secondly, mean transparency values range from 0.13 to 0.21. Both volcanic ash and Saharan dust patterns are less transparent than the lithogenic particles, the dust pattern was the least transparent. The superficial lithogenic particles are more transparent than the deeper samples. Roughness in the volcanic ash pattern showed the lowest value and particle sample E_10 the greatest. Mean and median roughness values are higher in the lithogenic particle samples than in the patterns except for the E1_20 sample. Edge gradient in the lithogenic particle samples show the least mean and median values.

Remarkably, this research work demonstrates the effectiveness of FlowCAM® analysis for textural studies of oceanic lithogenic particles and that the studied particles from the oceanic lithogenic flux samples contained a mix of both volcanic ash and Saharan dust grain size distribution patterns yet tend to resemble more the Saharan dust pattern.

ACKNOWLEDGEMENTS

Thank you to Dr. José Mangas Viñuela for his contribution on the mineralogy knowledge for this study, Dr. Javier Arístegui and his team for all the facilities provided to analyze the samples in the FlowCAM® and the ocean campaign PLOCAN and ULPGC members (Jose Joaquin Hernandez-Brito, Gabriel Juanes, Paula Pacheco, Raúl Jiménez, Iván Alonso, Néstor Rodríguez, Rayco Moran, Raúl Santana; Silvana Neves, Miguel Angel Gutierrez, Marta Veny, David Curbelo and Angel Rodríguez), that provided the collection of the analyzed oceanic samples in this work.

REFERENCES

- Anabalón, V., Arístegui, J., Morales, C.E., et al. 2014. The structure of planktonic communities under variable coastal upwelling conditions off Cape Ghir (31°N) in the Canary Current System (NW Africa). *Prog. Oceanogr.* 120: 320-339. <https://doi.org/10.1016/j.pocean.2013.10.015>
- Ancoechea, E. 2022. La erupción del volcán Cumbre Vieja, La Palma ¿qué hemos aprendido? Jornadas Telemáticas en la Real Academia de Ciencias Exactas, Físicas y Naturales. 22-23 marzo 2022. Online access: <https://youtu.be/NnYwBq4Dzaw>
- Armstrong R.A., Lee C., Hedges J.I., et al. 2002. A new, mechanistic model for organic carbon fluxes in the ocean: based on the quantitative association of POC with ballast minerals. *Deep-Sea Res. II* 49: 219-236. [https://doi.org/10.1016/S0967-0645\(01\)00101-1](https://doi.org/10.1016/S0967-0645(01)00101-1)
- Báez-Hernández M, García N, Menéndez I, Jaramillo A, Sánchez-Pérez I, Santana A, Alonso I, Mangas J, Hernández-León S. 2019. Interaction of sinking behaviour of Saharan dust and lithogenic and biogenic fluxes in the Canary Basin. *Scientia Marina* 83(2): 121-132 DOI: <https://doi.org/10.3989/scimar.04877.19A>
- Bishop, I.W., Spaulding S.A. 2017. Life cycle size dynamics in *Didymosphenia geminata* (Bacillariophyceae). *Journal of Phycology* 53: 652–663. <http://dx.doi.org/10.1111/jpy.12528>
- Blott, S.J. and Pye, K. (2001) GRADISTAT: a grain size distribution and statistics package for the analysis of unconsolidated sediments. *Earth Surface Processes and Landforms* 26, 1237-1248. <http://www.kpal.co.uk/gradistat.html>
- Buesseler K.O., Antia A.N., Chen M., et al. 2007. An assessment of the use of sediment traps for estimating upper ocean particle fluxes. *J. Mar. Res.* 65: 345-416. <https://doi.org/10.1357/002224007781567621>
- Carracedo, J.C., Pérez-Torrado, F., Rodríguez-González, A., Fernández-Turiel, J.L., Troll, V.R., Wiesmaier, S. 2022. The 2021 eruption of the Cumbre Vieja Volcanic Ridge on La Palma, Canary Islands. *Geology Today* 2022 38 (3), 94-107. <https://doi.org/10.31223/X5D06D>
- Carracedo, J.C., Rodríguez Badiola, E., Gouillou, H., De La Nuez, J., Pérez Torrado, F.J. 2001. Geology and volcanology of La Palma and El Hierro, Western Canaries. *Estudios Geológicos*, 57, 175-273.

- Dong, H.-P., Wang, D.-Z., Dai, M., et al. 2010. Characterization of particulate organic matter in the water column of the South China Sea using a shotgun proteomic approach. *Limnol. Oceanogr.* 55: 1565-1578. <https://doi.org/10.4319/lo.2010.55.4.1565>
- Elder, L.E., Hsiang, A.Y., Nelson K., et al. 2018. Data Descriptor: Sixty-one thousand recent planktonic foraminifera from the Atlantic Ocean. *Sci. Data* 5: 180109. <https://doi.org/10.1038/sdata.2018.109>
- Folk, R.L., Ward, W.C. 1957. Brazos River bar: a study in the significance of grain size parameters. *Journal of Sedimentary Petrology*, 27, 3-26.
- Frogner P., Gíslason S.R., Óskarsson N. 2001. Fertilizing potential of volcanic ash in ocean surface water. *Geology* 29 (6): 487–490. [https://doi.org/10.1130/0091-7613\(2001\)029<0487:FPOVAI>2.0.CO;2](https://doi.org/10.1130/0091-7613(2001)029<0487:FPOVAI>2.0.CO;2)
- Gómez-Letona, M., Arístegui, J., Ramos, A.G., Montero, M.F., Coca, J. 2018. Lack of impact of the El Hierro (Canary Islands) submarine volcanic eruption on the local phytoplankton community. *Scientific Reports* 8:4667 <http://doi.org/10.1038/s41598-018-22967-6>
- Goudie, A.S., Middleton, N.J., 2001. Saharan dust storms: nature and consequences. *Earth-Sci Rev.* 56, 179-204. [http://doi.org/10.1016/S0012-8252\(01\)00067-8](http://doi.org/10.1016/S0012-8252(01)00067-8)
- Holz, C., Stuut, J.B.W., Henrich, R., Meggers, H., 2007. Variability in terrigenous sedimentation processes off northwest Africa and its relation to climate changes: inferences from grain-size distributions of a Holocene marine sediment record. *Sediment. Geol.* 202 (3), 499-508. <https://doi.org/10.1016/j.sedgeo.2007.03.015>.
- Huskin I., Viesca L., Anadón R. 2004. Particle flux in the Subtropical Atlantic near the Azores: influence of mesozooplankton. *J. Plankton Res.* 26: 403-415. <https://doi.org/10.1093/plankt/fbh031>
- Jaramillo A., Menéndez I., Alonso I., Mangas J, Hernández-León S. 2016. Grainsize, morphometry and mineralogy of airborne input in the Canary basin: evidence of iron particle retention in the mixed layer. *Sci. Mar.* 80: 395-408.
- Mahiques, M.M. 2016. Sediment Sorting. In: Kennish, M.J. (eds) *Encyclopedia of Estuaries. Encyclopedia of Earth Sciences Series.* Springer, Dordrecht. https://doi.org/10.1007/978-94-017-8801-4_348
- Mangas J. 2022. Desde el manto terrestre hasta Cumbre Vieja (La Palma): La erupción volcánica de. *Macla* 26, 3-4.
- Menéndez I., Derbyshire E., Engelbrecht J., et al. 2009. Saharan dust and aerosols on the Canary Islands: past and present. In: Chang M., Liu W. (eds.), *Airborne Particulates*, Nova Publishers, New York, pp. 39-80.

- Menéndez, I., Derbyshire, E., Carrillo, T., Caballero, E., Engelbrecht, J. P., Romero, L. E., Mayer, P. L., Rodríguez de Castro, F., Mangas, J. 2017. Saharan Dust and the impact on adult and elderly allergic patients: the effect of threshold values in northern sector of Gran Canaria, Spain. *International Journal of Environmental Health Research*, 27 (2), 144-160. <http://doi.org/10.1080/09603123.2017.1292496>
- Menéndez, I., Díaz-Hernández, J.L. Mangas, J., Alonso, I., Sánchez, P.J., Soto, 2007. Airborne Dust accumulation and soil development in the North-East sector of Gran Canaria, Canary Island, Spain. *Journal of Arid Environments* 71, 57-89. <http://doi.org/10.1016/j.jaridenv.2007.03.011>
- Milliman, J.D., Syvitsku, J.P.M. 1992. Geomorphic/Tectonic control of sediment discharge to the ocean: The importance of Small Mountainous Rivers. *Journal of Geology* 100: 525-544.
- Pankhurst, M.J.; Scarrow, J.H.; Barbee, O.A., Hickey J.; Coldwell, B.C.; Rollinson, G.K.; Rodríguez-Losada, J.A.; Mar-tín-Lorenzo, A.; Rodríguez, F.; Hernández, W.; Calvo-Fernández, D.; Hernández, P.; Pérez, N.M. 2022. Rapid response petrology for the opening eruptive phase of the 2021 Cumbre Vieja eruption, La Palma, Canary Islands. Preprint, Research Square <https://doi.org/10.21203/rs.3.rs-963593/v1>
- Piqué, A. 2001. *Geology of Northwest of Africa*. Gebrüder Borntraeger, Berlin.
- Poulton, N.J. 2016. FlowCam: Quantification and Classification of Phytoplankton by Imaging Flow Cytometry. In: Barteneva, N., Vorobjev, I. (eds) *Imaging Flow Cytometry. Methods in Molecular Biology*, vol 1389. Humana Press, New York, NY. https://doi.org/10.1007/978-1-4939-3302-0_17
- Ratmeyer V., Fischer G., Wefer G. 1999. Lithogenic particle fluxes and grain size distributions in the deep ocean off northwest Africa: Implications for seasonal changes of aeolian dust input and downward transport. *Deep Sea Research Part I: Oceanographic Research Papers* 46:1289-1337.
- Sangrà P., Pascual A., Rodríguez-Santana A., et al. 2009. The Canary Eddy Corridor: a major pathway for long-lived eddies in the North Atlantic. *Deep-Sea Res I* 56: 2100-2114. <https://doi.org/10.1016/j.dsr.2009.08.008>
- Schmincke, H.U., Sumita, M., 2010. *Geological Evolution of the Canary Islands: A Young Volcanic Archipelago Adjacent to the Old African Continent*. Ed. Görres, Koblenz (200 pp).
- Spaulding S.A., Jewson D.H., Bixby R.J., Nelson H., McKnight D.M. 2012. Automated measurement of diatom size. *Limnology and Oceanography: Methods* 10: 882–890. <http://dx.doi.org/10.4319/lom.2012.10.882>

Sprengel C., Baumann K.-H., Neuer S. 2000. Seasonal and interannual variation of coccolithophore fluxes and species composition in sediment traps north of Gran Canaria (29°N 15°W). *Mar. Micropaleontol.* 39: 157-178. [https://doi.org/10.1016/S0377-8398\(00\)00019-0](https://doi.org/10.1016/S0377-8398(00)00019-0)

Van der Does, M., Wengler, M., Lamy, F., Martinez-Garcia, A., Jaccard, S.L. et al. 2021. Opposite dust grain-size patterns in the Pacific and Atlantic sectors of the Southern Ocean during the last 260,000 years. *Quaternary science reviews* 263: 106978 <https://doi.org/10.1016/j.quascirev.2021.106978>

Lava deltas photos: <https://n.com.do/2021/11/13/una-playa-canaria-queda-sepultada-bajo-la-lava-del-volcan-de-la-palma/>

<https://ondacerolapalma.com/las-coladas-1-y-2-se-unen-formando-una-unica-fajana-que-ha-sepultado-la-playa-de-los-guirres-y-el-kiosco/>

1. ACTIVIDADES DESARROLLADAS DURANTE LA REALIZACIÓN DEL TFT

Los datos para la realización de este TFT se obtuvieron todos a partir del trabajo hecho durante las prácticas externas. En estas prácticas, utilicé la FlowCAM® para analizar muestras de partículas de flujo litogénico oceánico en la costa de la isla de La Palma durante la erupción del volcán de 2021. A partir de estas muestras se realizó un tratamiento de datos para obtener una gráfica de distribución de tamaños en la que se comparaban las muestras de agua recogidas con dos patrones, uno de polvo Sahariano y otro de ceniza volcánica del volcán mencionado y así poder observar cuanto influía este nuevo aporte de partículas al flujo litogénico de la columna de agua de la costa de La Palma. También se obtuvieron datos de mineralogía de las partículas estudiadas.

2. FORMACIÓN RECIBIDA

Para ver las imágenes de las partículas captadas por la FlowCAM® solo puede utilizarse un programa llamado VisualSpreadSheet, el cual mi co-tutora me enseñó a usar. Tuve que aprender mucho sobre este programa, como calculaba, como guardaba las imágenes, como crear librerías, etc., para luego así poder distribuir y ordenar las imágenes que me interesaban y las que no para luego poder pasar al tratamiento de datos. Para la caracterización mineralógica de las partículas se utilizaron diferentes parámetros estadísticos. Para su cálculo utilicé una hoja de cálculo (gradistrat) la cual mi tutora me enseñó a usar.

3. INTEGRACIÓN, IMPLICACIÓN Y RELACIÓN CON EL PERSONAL

Mi integración fue muy buena, todos los trabajadores de la institución estaban dispuestos a ayudar, y tenerlos alrededor amenizaba las horas de trabajo gracias a su compañía. La implicación fue muy buena también, desde el primer momento estuve trabajando con mucho esfuerzo y motivación. La relación con el personal fue perfecta, en ningún momento hubo ningún problema.

4. ASPECTOS POSITIVOS Y NEGATIVOS

El mayor aspecto positivo es que trabajamos sobre un evento muy reciente e importante como es la erupción del volcán de La Palma, que ocurrió hace menos de un año y por lo tanto aportamos información nueva al mundo de la ciencia, un estudio que todavía nadie ha realizado y además, con un método que tampoco nunca antes se había probado ya que la FlowCAM® está hecha para analizar partículas biogénicas. Esto también tiene un aspecto negativo ya que, al no existir otros artículos con esta información, no pudimos respaldar ciertos datos.

5. VALORACIÓN PERSONAL DEL APRENDIZAJO CONSEGUIDO

Estoy muy orgulloso de todo lo que he conseguido con este TFT, después de los meses de esfuerzo considero que he conseguido integrarme un paso más dentro del mundo de la ciencia.

**FLOWCAM ANALYSIS OF THE OCEAN LITHOGENIC PARTICLES DURING THE 2021
VOLCANIC ERUPTION OF LA PALMA, CANARY ISLANDS**

Eduardo Augustin Baixas